CHAPTER V
RESULTS AND DISCUSSION

In this chapter, the results of following physical properties of the commercial adsorbents are presented: Static adsorption capacity using the thermogravimetric analyzer (TGA), and crystallinity patterns using the X-ray diffraction analysis.

Moreover, the adsorption isotherm determined from the entire bed of the multi-layer adsorber was established. In addition, the breakthrough curve behaviors of the adsorption of water onto the multi-layer adsorber at various humidity levels and contact times are discussed and reported. Finally, the theoretical breakthrough curves predicted from the mathematical model are proposed in this chapter.

5.1 Adsorbent Characterization

5.1.1 Static Adsorption Capacity

The capacity of the adsorbent for water is normally expressed in mass of adsorbed water per mass of adsorbent (Campbell, 1992). The term of static adsorption capacity is the water capacity of new or virgin adsorbent as determined in an equilibrium cell with no fluid flow (Campbell, 1992). It is an indicator to measure the ability of fresh adsorbent in removing the water vapor from the bulk gas and storing that amount of water inside.

The comparison of water adsorption capacity estimated from the TGA is shown in Table 5.1. The silica gel adsorbent presents the highest adsorption capacity because it has the highest pore volume among all adsorbents analyzed. In another words, all the voids of the silica gel adsorbent are nearly filled up.

In addition, the difference between the adsorption capacities of the MolSiv (zeolite) Type 4A with the pellet sizes of 1/8" and 1/16" are similar, and much smaller than that of silica gel. It could be implied that the size of pellets has no effect on static adsorption capacity of MolSiv 4A because water adsorption capacity of the MolSiv (zeolite) is normally dependent on the total pore volume created from crystalline cavity.

Moreover, the static adsorption capacity reported in Table 5.1 is very close to the pore volume presented in Howe-Grant and Kroschwitz (1992). This result supported the aforementioned assumption that the adsorption capacity increased with increasing pore volume.

Table 5.1 Static adsorption capacity of fresh adsorbent at 100%RH and 25°C

Adsorbent Type	**Adsorption Capacity for Water (g H_2O/100 g adsorbent)**
Silica gel	39.96
MolSiv (Zeolite) Type 4A with nominal pellet size 1/8" †	28.07
MolSiv (Zeolite) Type 4A with nominal pellet size 1/16" †	29.33

†The pellet size is in an extruded (cylindrical) shape, and the nominal pellet size represents a spherical adsorbent with volume equivalent to that of cylindrical adsorbent

Figure 5.1 illustrates the TGA results for silica gel adsorbent. The maximum weight loss occurred at the temperature of around 75°C, obviously indicated by the derivative peak where the large portion of water was desorbed from the adsorbent pellets. At the temperatures of above 150°C, the change in percentage of weight remaining was very slow and remained flat, implying that the total amount of water had been already desorbed. On the other hand, in order to regenerate the Silica gel adsorbent effectively, the temperatures of above 150°C are required.

The amount of adsorbed water can be determined from the area under the derivative peak. The comparison of derivative weight loss on the silica gel powder and the silica gel pellet is depicted in Figure 5.2. The derivative peak of silica gel powder is presented at slightly lower temperature than that of the pellet, implying that the adsorbed water could be desorbed from the powder type faster than the pellet type because the smaller particle size provides better heat transfer rate and/or area.

Moreover, the higher contact area not only contributes the better heat transfer rate but also the higher mass rate of water being adsorbed on or desorbed from the adsorbent.

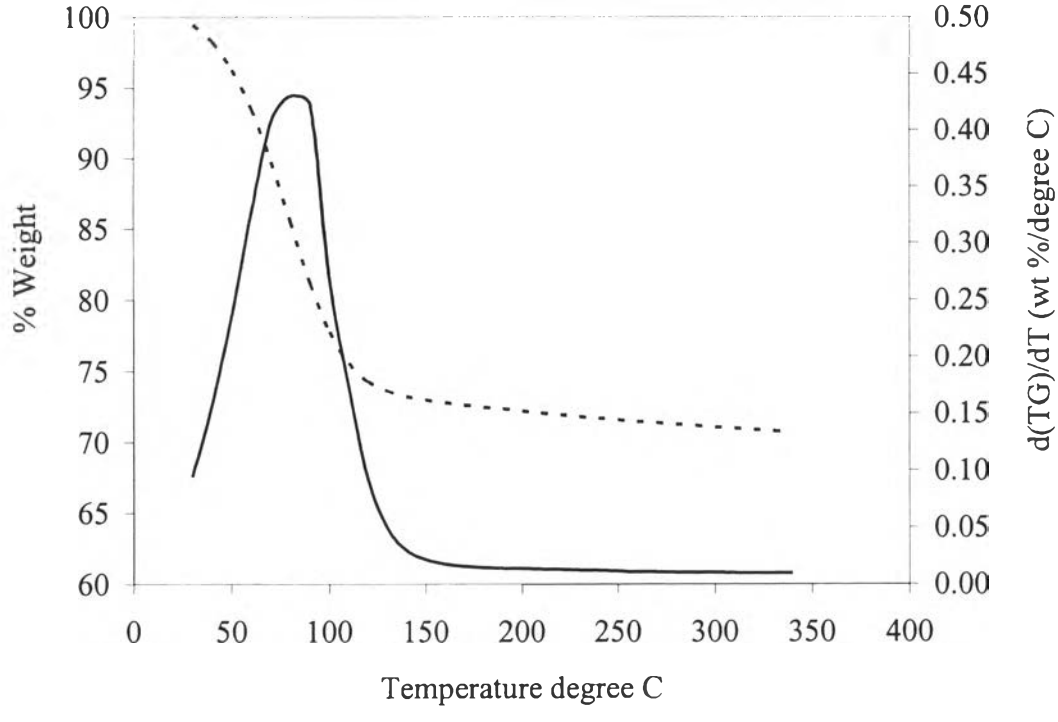

Figure 5.1 Weight loss of water saturated on silica gel adsorbent from TGA experiment: %Weight(---), and Weight loss derivative (—).

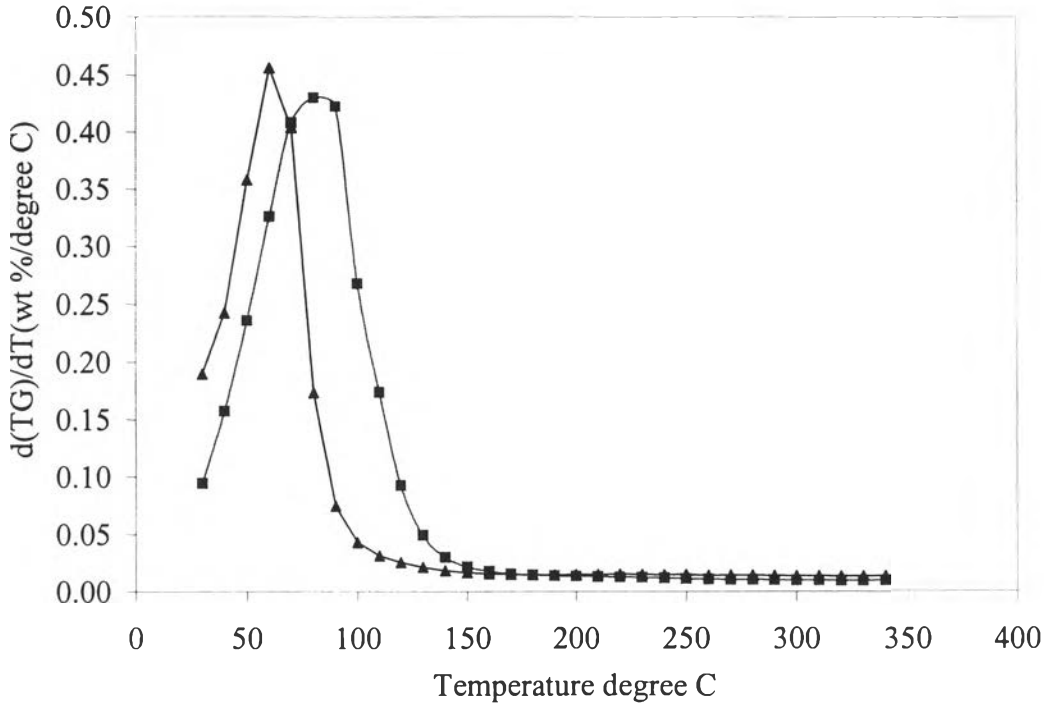

Figure 5.2 Comparison of weight loss on the pellet and the powder of silica gel adsorbents: Pellet(■), and Powder(▲).

The TGA results of MolSiv 4A with the pellet size of 1/8" and 1/16", as shown in Figure 5.3, exhibit two derivative peaks at the temperatures of around 50°C and 150°C. At the first derivative peak, the water was desorbed from the surface of the adsorbent or from the macro-pores. Since the commercial materials were prepared as pellet agglomerates containing a high percentage of the crystalline zeolite together with an inert binder, these agglomerates introduced the macro-pores into the pellet (Rousseau, 1987). At the higher temperature where the second derivative peak appeared, the water was then desorbed from the voids within the zeolite crystal (crystalline cavity).

Because the polarity force between the water and the zeolite's crystal structure is relatively strong, the regeneration of this type of adsorbent requires relatively high temperature.

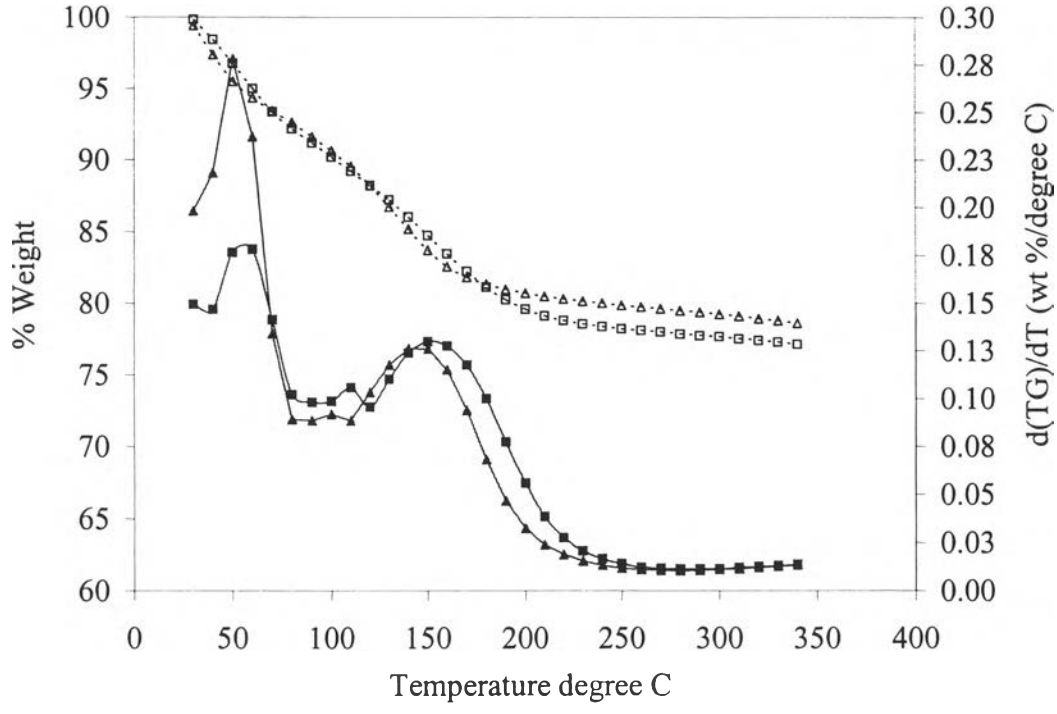

Figure 5.3 Weight loss of water saturated on 1/8"(□), and 1/16"(△) MolSiv 4A, and weight loss derivative on 1/8"(■), and 1/16"(▲) MolSiv 4A.

In addition, at the temperature above 250°C, the percentage of weight remaining dropped very slowly because there was only little amount of water left in the pores. Therefore, the temperatures of above 250°C are required to regenerate the MolSiv 4A effectively. Typically, MolSiv 4A is regenerated at 350°C.

Although the silica gel has higher adsorption capacity, it has weaker adsorption force compared with the MolSiv 4A because the structure of the silica gel offers lesser polarity force to water, or lesser water affinity than that of the MolSiv 4A. The TGA derivative peak in Figure 5.1 indicates that the water was desorbed from the silica gel at the lower temperature than that of the MolSiv 4A in Figure 5.3. As a result, the MolSiv 4A adsorbent requires higher temperature for the regeneration than the silica gel adsorbent.

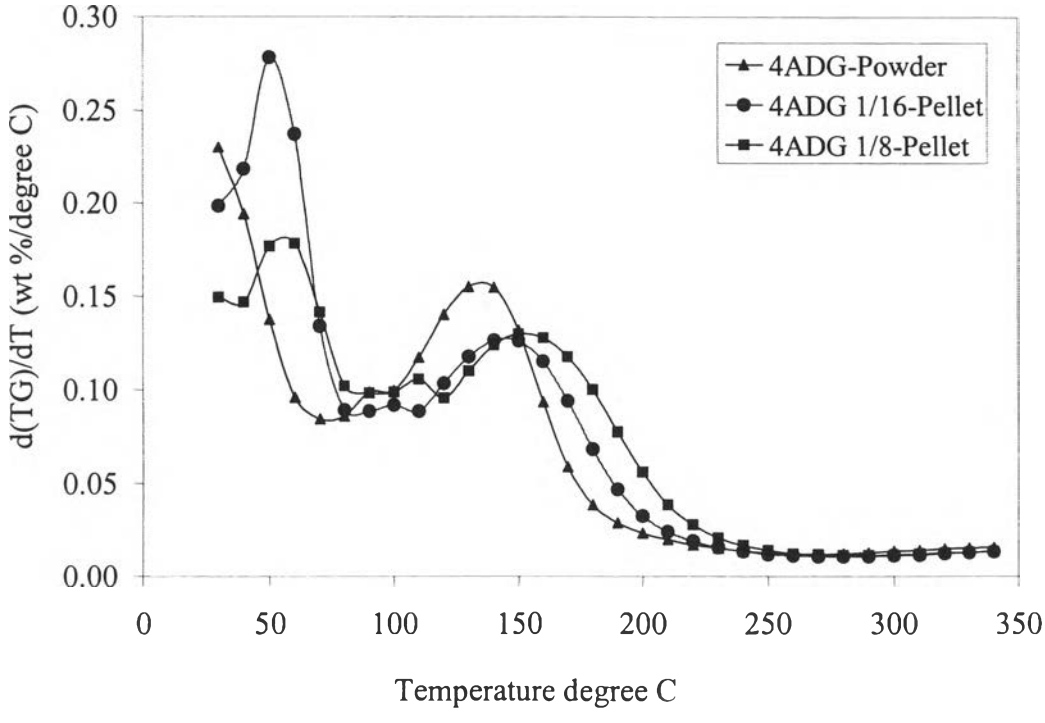

Figure 5.4 Comparison of weight loss derivative on three different sizes of MolSiv 4A: 1/8"(■), 1/16"(▲), and Powder (●).

The size of the adsorbents has an effect upon the heat transfer area and the weight-loss-derivative curves. From Figure 5.4, the larger particle size, which has lesser heat transfer area, would cause the weight-loss-derivative curve to be shifted to the right-hand side or to higher temperature. On the other hand, the smaller the particle size is, the larger the heat transfer area is, and the lower the temperature is required for regeneration. As a result, in order to achieve better heat and mass transfer areas, the adsorbent should be always the smallest comparable with the pressure drop limitation (Campbell, 1992).

5.1.2 X-ray Diffraction Pattern

The X-ray Diffraction (XRD) pattern of the commercial silica gel adsorbent in Figure 5.5 indicates an amorphous solid structure whereas the XRD pattern of the commercial MolSiv 4A represents a highly crystallized structure as shown in Figure 5.6. Obviously, both MolSiv 4A with pellet sizes of 1/8" and 1/16"

have exactly the same XRD patterns. In the experiment, the MolSiv 4A with pellets of 1/8" and 1/16" were used in the middle and the bottom layers of a multi-layer adsorber, respectively.

However, it is very difficult to provide additional detailed investigation on the influence from the structure of the commercial zeolite adsorbents because of the complexity of its structure. Consequently, there is no analysis report for the composition of the zeolite adsorbent.

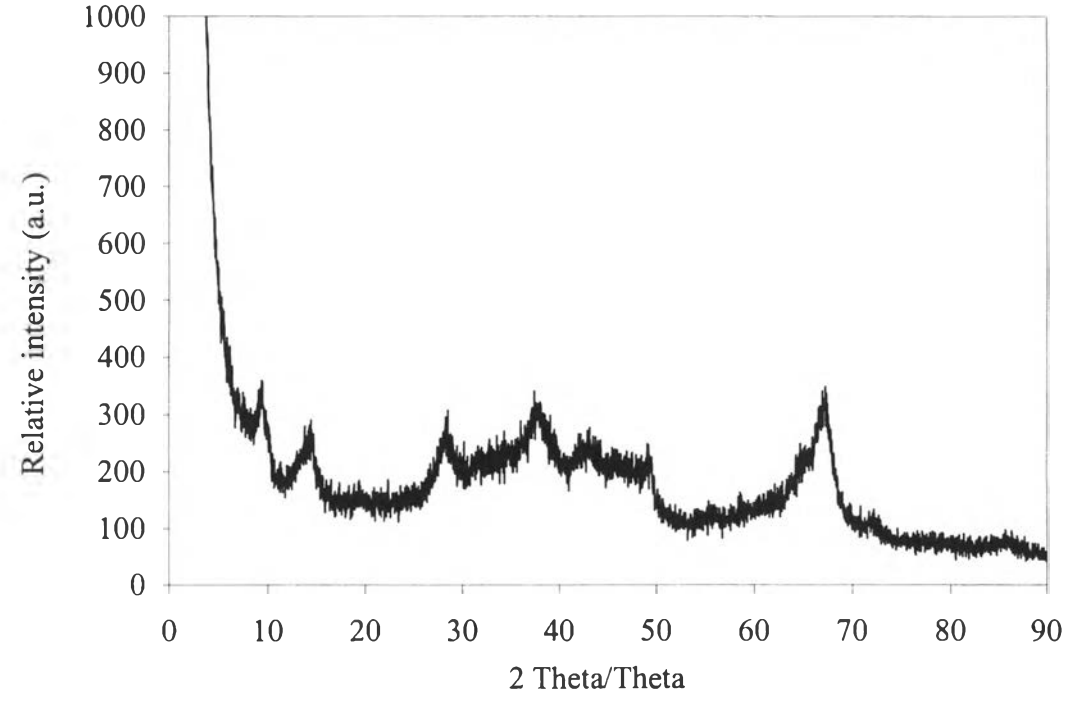

Figure 5.5 X-ray Diffraction pattern of fresh silica gel adsorbent.

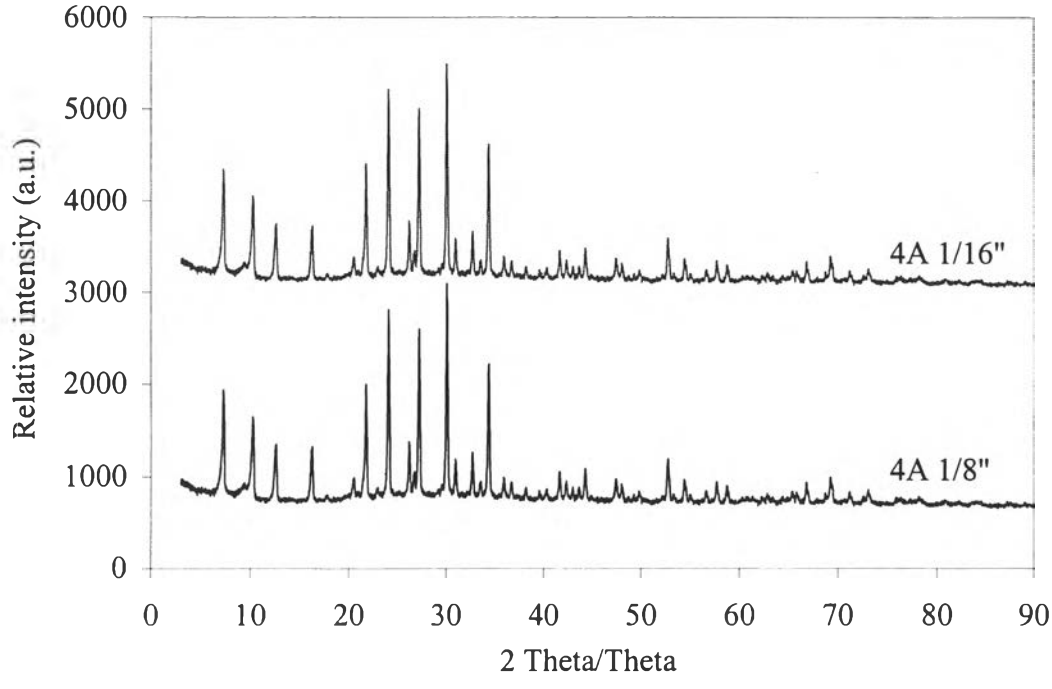

Figure 5.6 X-ray Diffraction pattern of fresh MolSiv 4A with the pellet sizes of 1/8" and 1/16".

5.2 Adsorption Isotherm

The equilibrium adsorption isotherm for water on a multi-layer adsorber at 25°C, and 1 atm shows a slight upward curve pass the plateau representing monolayer coverage as shown in Figure 5.7. This adsorption isotherm result might be mainly dominated by the 96 % by volume of MolSiv 4A with 1/8" and 1/16" pellets only, or a combination of all adsorbents (MolSiv 4A with 1/8" and 1/16" pellets and Silica gel).

Supposing the former assumption above was true, the adsorption isotherm results should be possibly analogous to the Type II Brunauer isotherm or the Sigmoid or S-shaped isotherm, and this might indicate that there was a continuous progression with increasing loading from monolayer to multilayer and, then, to capillary condensation (Ruthven, 1984). Moreover, this may indicate that more water molecules were adsorbed even after the first layer was filled. Although the

multilayer adsorption and capillary condensation are generally observed only in adsorbents with a wide range of pore sizes (Ruthven, 1984).

The Kelvin equation, in Appendix H, explains how it is possible for water to condense inside of zeolite. According to the Kelvin equation, the capillary condensation occurs because the saturation water vapor in a small pore is reduced by the effect of high surface tension (Dobson, 1987). As a result, the small pores will be completely filled with liquid water. Additionally, the capillary condensation may occur inside the macro-pores of the zeolite pellet at high humidity.

Furthermore, the slight upward curve present at higher humidity might be an effect of the silica gel. Since, the silica gel has higher adsorption capacity at higher humidity, as a result the higher average adsorption capacity of the entirely bed was observed. In addition, this gain capacity might be involved from the pore condensation on silica gel. However, only 4% by volume of the silica gel, the adsorption capacity at this stage shown a little increased

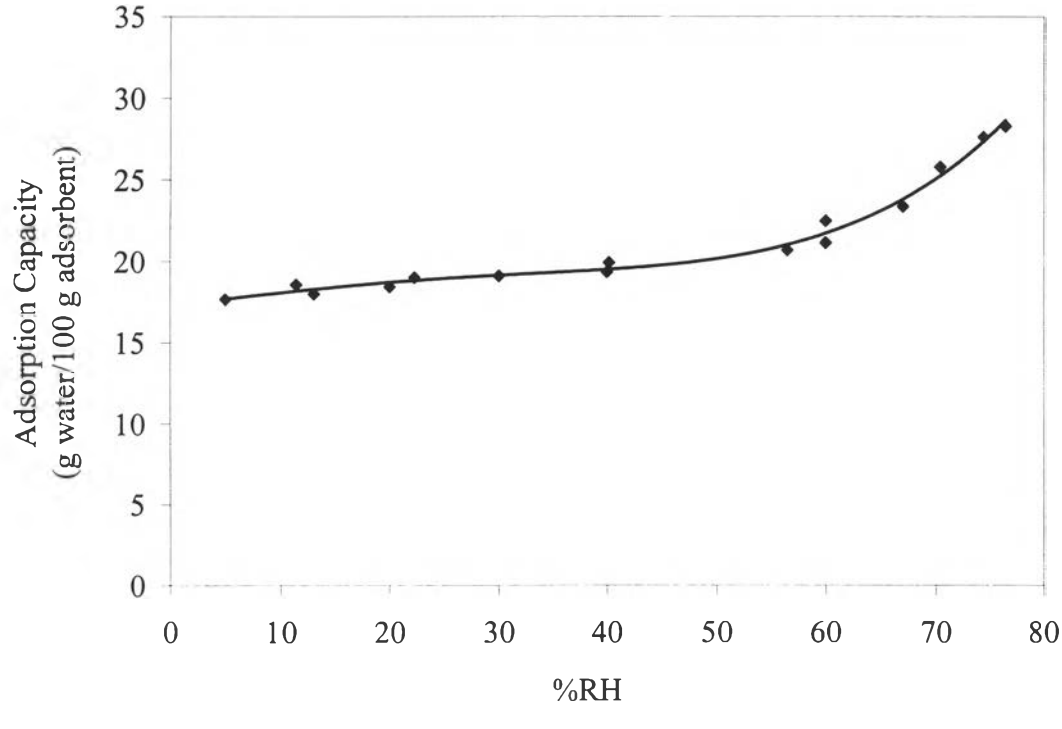

Figure 5.7 Equilibrium adsorption isotherm of water on the multi-layer adsorber at 25 °C, and 1 atm.

5.3 Adsorption Breakthrough Curves

5.3.1 Effects of Humidity Level in Natural Gas Feed on Breakthrough Curves

The first two experiments were carried out to investigate the effects of humidity level in the natural gas feed on the shape of the breakthrough curves under two different humidity levels at 76.44%RH and 65.00%RH with the constant feed flow rate of 130 ml/min, which was equivalent to the contact time of 34 seconds.

Two different operating conditions resulted in two breakthrough curves as shown in Figure 5.8. Due to the display limitation of humidity analyzer, the breakthrough point criterion used in the experiments was limited at 0.1%RH (the minimum display resolution) at the end of the adsorber. When the humidity levels of the inlet gas were 60%RH and 76.44%RH, the amount of time consumed for the outlet water concentration to start appearing was about 65 hours and 59 hours, respectively. With the criterion, the points at time consumed represented the breakthrough points or breakthrough times for the two conditions. In addition, the acceleration of the water breakthrough time was observed with an increase in humidity level of the natural gas feed.

Additionally, while the humidity in the outlet gas stream increased from zero, it indicated that the mass transfer zone was approaching to the exit of the column because the adsorbents continued to be nearly completely saturated.

A decrease in the slope at the end of the breakthrough curve implied that the adsorbents still had some remaining adsorption capacity to be able to adsorb more water. Noticeably, the slope tends to be flatter when the humidity of the feed is higher. At this stage, the silica gel had played an important role in this further water adsorption due to its higher adsorption capacity and capillary condensation effect. Referred to the preceding paragraph of the equilibrium adsorption isotherm in Figure 5.7, it was presumably described that although the adsorbents were nearly completely saturated, the adsorption capacity would keep the adsorption activity a little further ongoing due to multilayer adsorption or pore condensation. Therefore, the higher adsorption capacity of the whole bed appeared at higher humidity in the inlet, or at the end of the equilibrium adsorption isotherm depicted in Figure 5.7.

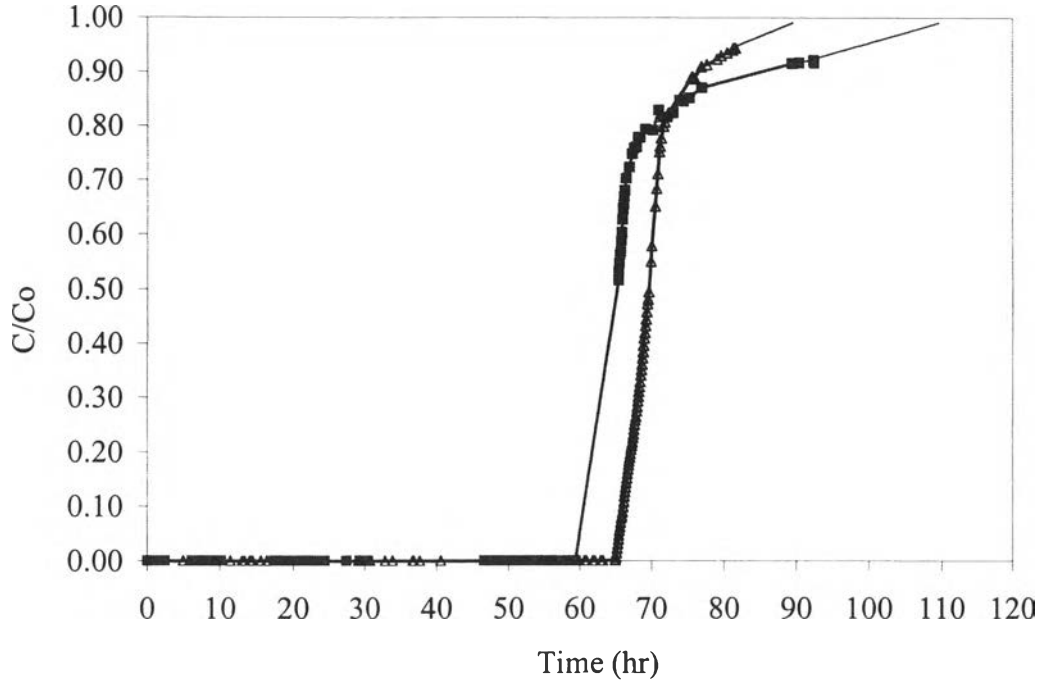

Figure 5.8 Effects of humidity levels in natural gas feed on breakthrough curves at the contact time of 34 sec: 60%RH (△) and 76.44%RH (■).

5.3.2 Effects of the Contact Time on Breakthrough Curves

It was clear to observe the effect of the contact time on the breakthrough time in Figure 5.9. At the same humidity level of 60%RH, the breakthrough time was inversely proportional to the contact time. On the other hand, an increase in the feed flow rate or a decrease in the contact time resulted in a decrease in or an acceleration of the breakthrough time. A similar results was also discussed by Chern and Chien (2001). This acceleration of the breakthrough time resulted from higher water loading.

Furthermore, the similarity of two breakthrough curve patterns implied that there was no significant effect of the feed concentration and contact time in the experiments on the pattern of the breakthrough curves. In addition, the steep breakthrough curve indicated that the sharp separation took place in the column resulted from the effect of a small adsorbent size (Campbell, 1992).

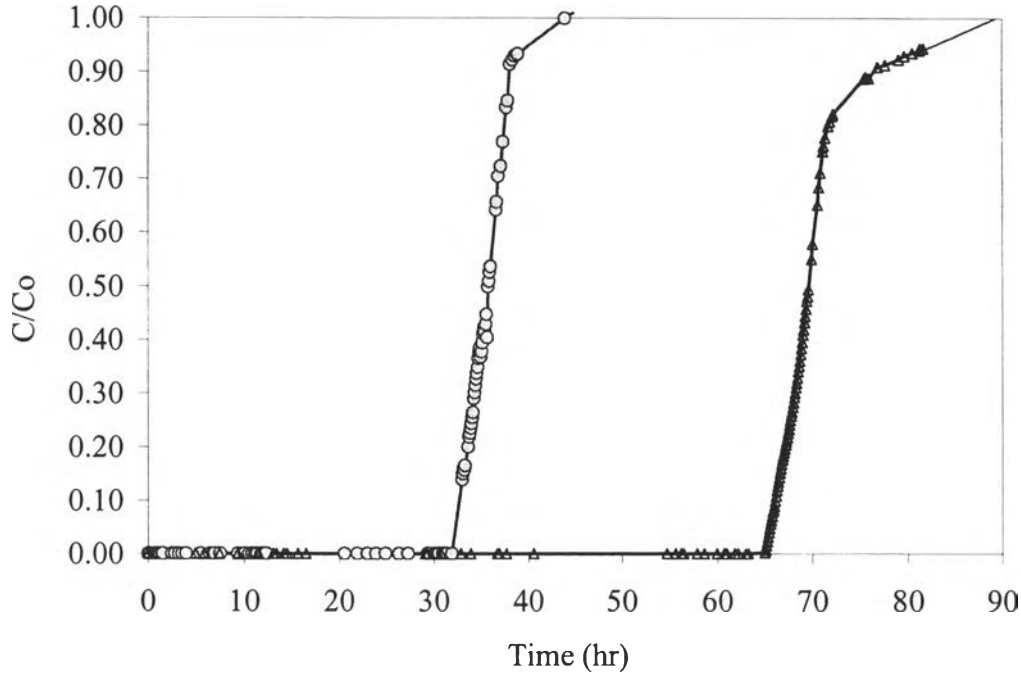

Figure 5.9 Effects of contact time (or feed flow rate) on breakthrough time at the same humidity level of 60%RH; 17 sec (●) and 34 sec (△).

The summary of the dynamic adsorption capacity at various humidity levels and contact time is shown in the Table 5.2. Since the partial pressure of water vapor (as humidity) is directly proportional to the driving force of the mass transfer between fluid-phase and solid-phase, in case the humidity level of the feed inlet decreases, the adsorption capacity is decreased as well. For an example in Table 5.2, at the same operating conditions, with lower inlet humidity levels of Run 2 compared to that of Run 1, the dynamic adsorption capacity of Run 2 is lower. Theoretically, the driving force model in Equation (4.5) can be used to explain this effect.

Table 5.2 Operating conditions and dynamic adsorption capacity obtained from two different humidity levels

Description	Unit	Run#1	Run#2	Run#3
Total adsorbent weight (dry)	g	49.50	49.50	51.83
Inlet water concentration	%RH	76.44	60.00	60.00
Gas flow rate	ml/min	130.00	130.00	260.00
Contact time	sec	34.00	34.00	17.00
Average inlet temperature	°C	25.33	24.98	25.15
Estimated Breakthrough point @ start to saturate	hr	59.42	65.08	31.90
Dynamic Adsorption Capacity	g H_2O/100 g adsorbent	28.31	21.14	22.48

5.4 Mathematical Models for the Adsorption on a Multi-layer Adsorber

5.4.1 Equilibrium Adsorption Isotherm Model

The equilibrium adsorption isotherm from the experiment was separated into two regions. The first region contained a range of data points at humidity level from 0%RH to 52 %RH whereas the second region accommodated the data points at the humidity level of above 52%RH. The equilibrium adsorption model which is analogous to the Langmuir model established a good correspondence with the experimental data points in the first region whereas the Linear model and the Freundlich model demonstrated a good representative of the experimental data points in the second region. These equilibrium adsorption models were further applied to the mathematical model for theoretical breakthrough curves, which was discussed later in this chapter. The equilibrium adsorption constants for three models are presented in Table 5.3. All the constants were obtained by using a regression technique in the Polymath program. Due to the limitations of experimental apparatus, the data at low humidity levels had to be extrapolated.

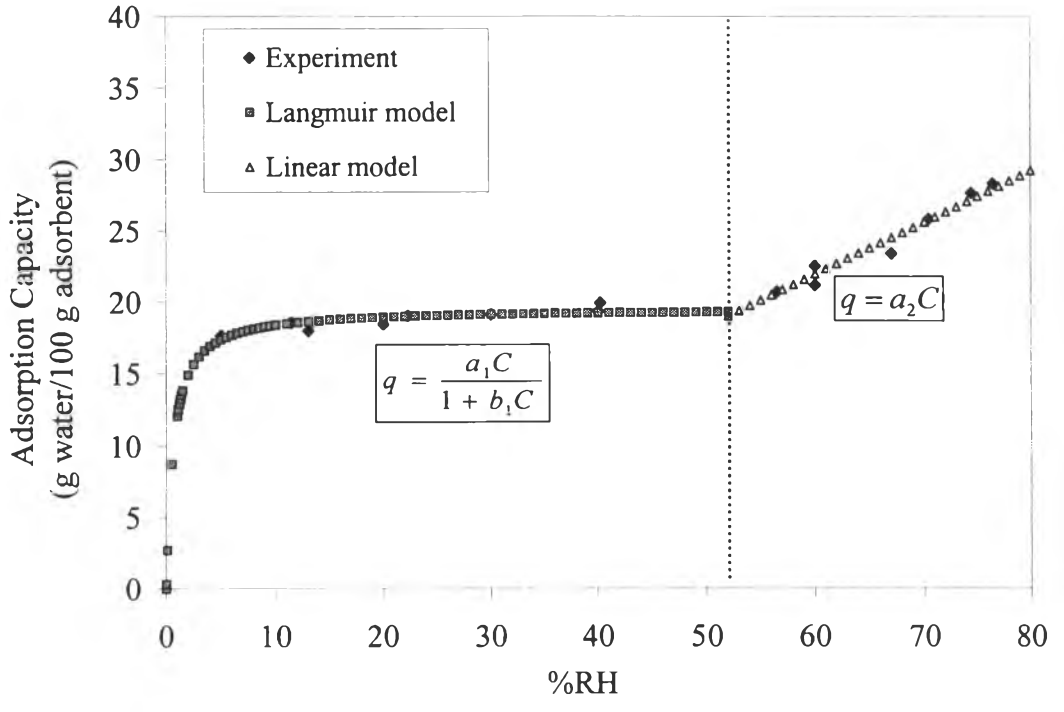

Figure 5.10 Equilibrium adsorption models for the multi-layer adsorber.

Table 5.3 Constants for adsorption isotherm equations

Region	Model	Equation ‡	Constant	
1	Langmuir	$q = \frac{ac}{1+bc}$	a	2.4655E+06
			c	1.2637E+05
			r^2	0.9955
2	Linear	$q = ac$	a	2.8557E+04
			r^2	0.9420
	Freundlich	$q = ac^n$	a	2.4167E+04
			n	0.9764
			r^2	0.9418

‡ concentration in mol/l

5.4.2 Theoretical Breakthrough Curves

The dynamic adsorption model was developed using both mass transfer and adsorption theories to investigate the adsorption of water vapor from the natural gas onto the multi-layer adsorber. The parameters utilized in the model were treated as the effective values in order to cover all gas and adsorbent properties. The dynamic adsorption equilibrium model obtained from the experiment was also applied and the Linear Driving Force model (LDF) was used to represent the mass transfer rate. Moreover, this LDF model was a lumped model to account the overall mass transfer between the bulk fluid phase and solid adsorbent phase.

In addition, the following assumptions were applied to the mathematical model to obtain the theoretical breakthrough curves:

- negligence of competitive adsorption by other components,
- unsteady state mass transfer,
- axial dispersion plug flow,
- constant fluid velocity, and
- isothermal system.

The FORTRAN computer language was employed to solve the mathematical model for the adsorption breakthrough curves at various conditions (Appendix G).

Effect of Effective Overall Mass Transfer Coefficient (k_e) on Theoretical Breakthrough Curves

The result of the mathematical model was practically dependent on the approximate value of the mass transfer coefficient (k or k_e). In order to obtain the best agreement between the experimental and mathematical adsorption breakthrough curves, k_e was necessary to be adjusted. According to the Figure 5.11 and 5.12, the theoretical breakthrough curves were very sensitive to k_e. An increase in k_e not only generated steeper curves, but also extended the breakthrough time. The mass transfer coefficient, k_e is the representative of the mass transfer rate from the gas phase to the adsorbent phase; therefore, the uptake rate of water by adsorbent is directly proportional to k_e.

From the theoretical breakthrough curves in the Figure 5.11 to 5.15, when k_e was about $1.0x10^{-4}$, the theoretical breakthrough pattern appeared to be similar to the experimental shape, but the breakthrough time was quite different from the experiment values. With k_e above $1.5x10^{-4}$, although the theoretical breakthrough time tended to be closer to the experimental values, the breakthrough patterns started to dissimilate from the experimental ones. As a result, it was implied that k_e was mathematically constrained to be not exceeding $1.5x10^{-4}$. By above reasonable assumptions, the k_e value of around $1.0x10^{-4}$ was practically acceptable for all case scenarios of the experiments.

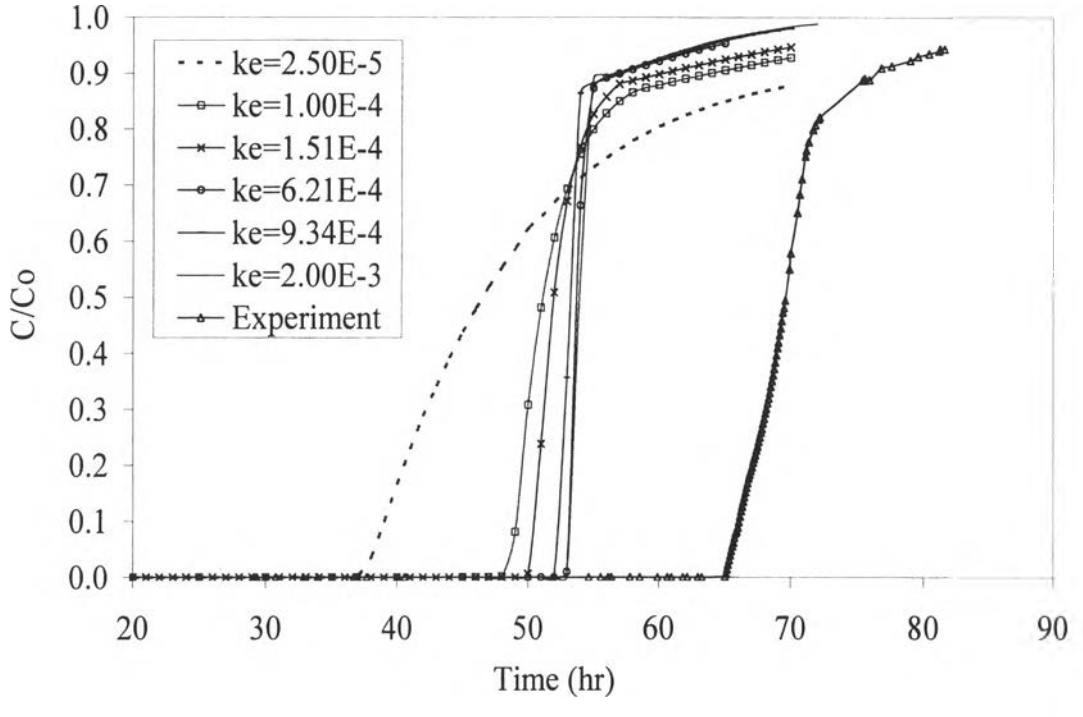

Figure 5.11 Effect of mass transfer coefficient (k_e) on theoretical breakthrough curves at the contact time of 34 sec and the feed humidity of 60%RH.

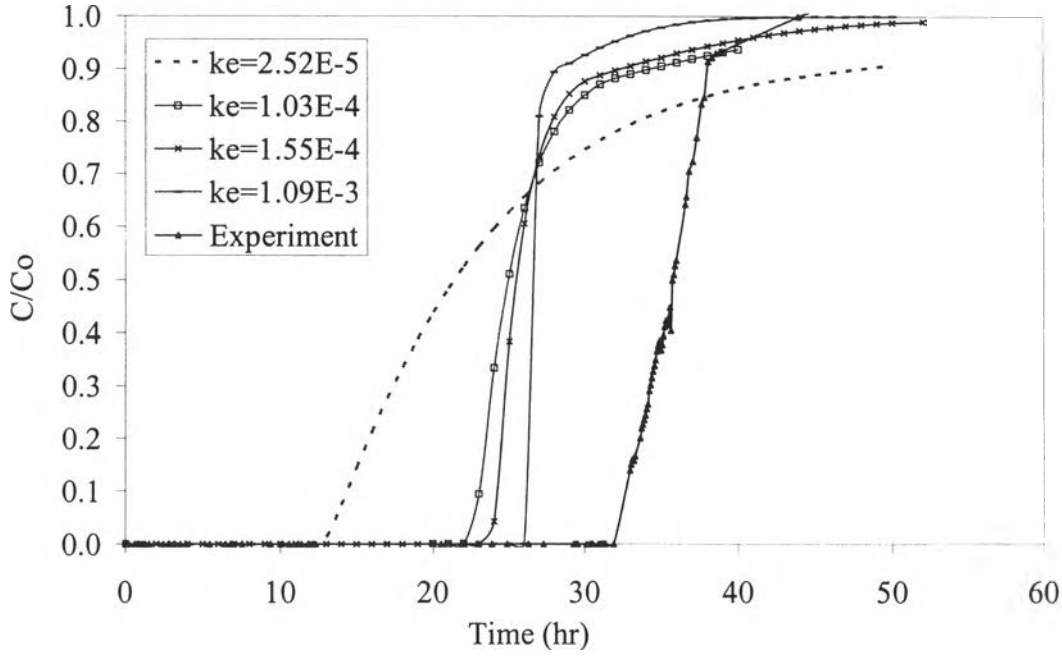

Figure 5.12 Effect of mass transfer coefficient (k_e) on theoretical breakthrough curves at the contact time of 17 sec and the feed humidity of 60%RH.

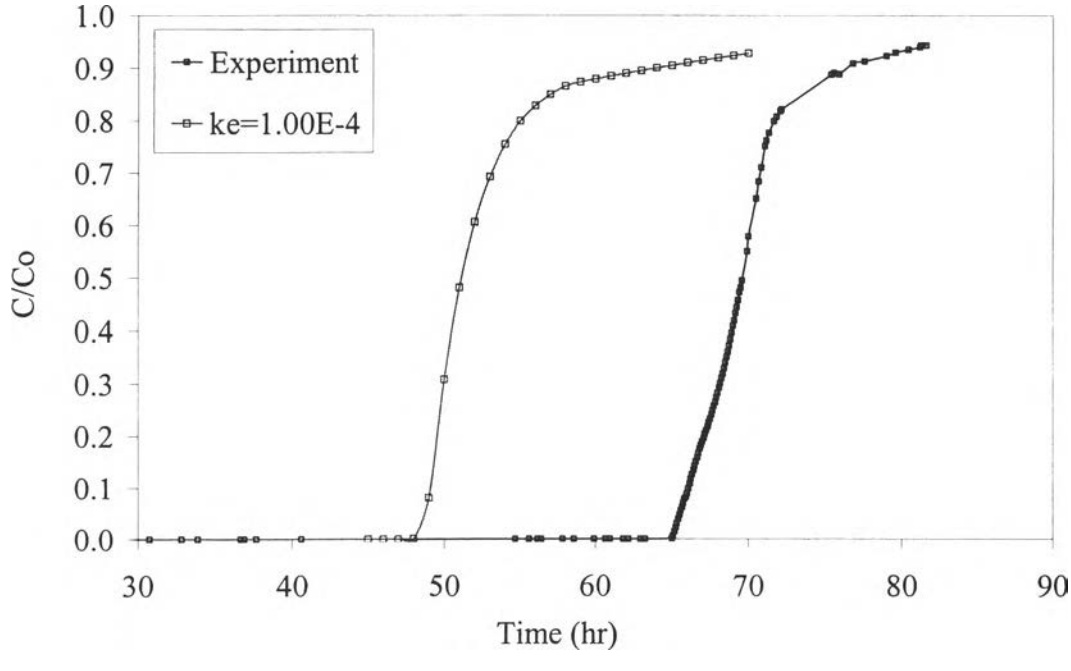

Figure 5.13 Experimental and theoretical breakthrough curves at the contact time of 34 sec, the feed humidity of 60%RH, and k_e of 1.00E-4.

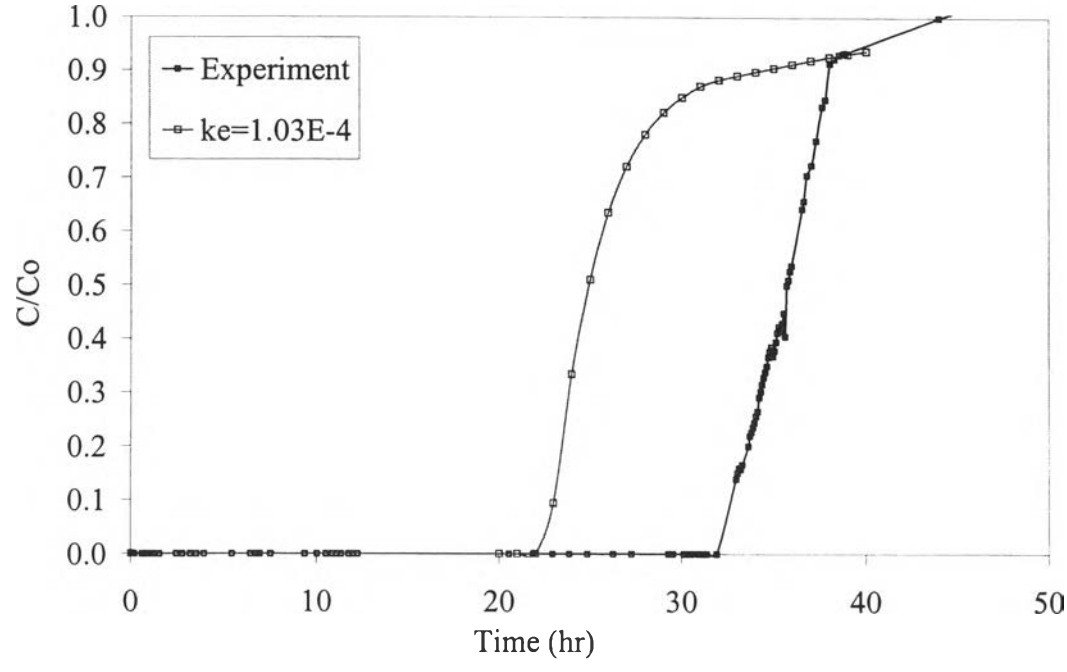

Figure 5.14 Experimental and theoretical breakthrough curves at the contact time of 17 sec, the feed humidity of 60%RH, and k_e of 1.00E-4.

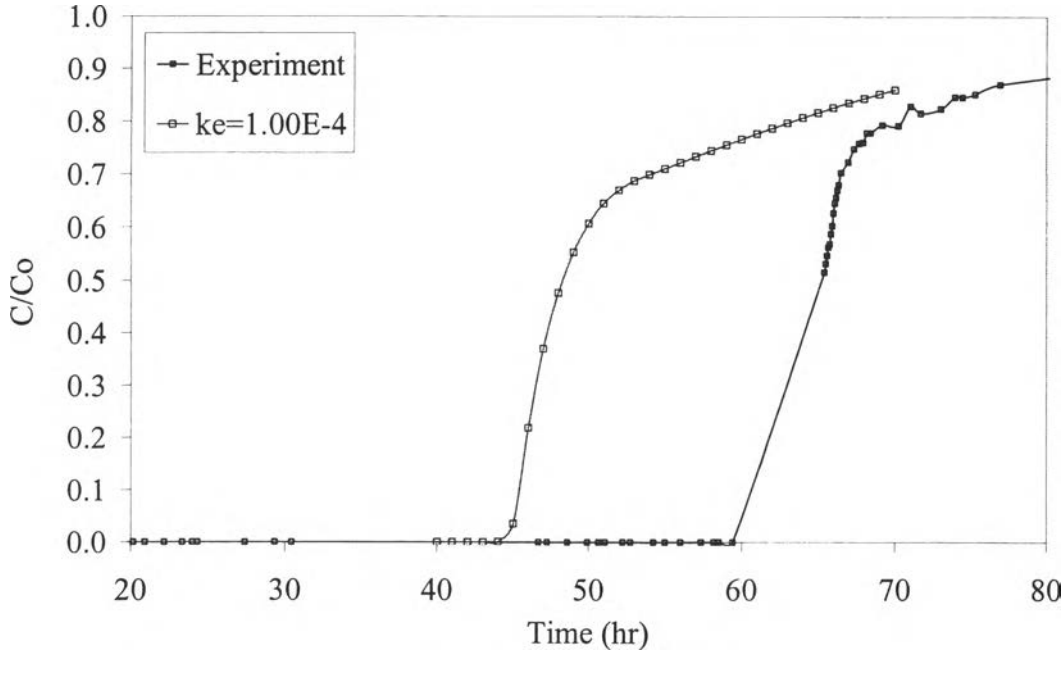

Figure 5.15 Experimental and theoretical breakthrough curves at the contact time of 34 sec, the feed humidity of 75%RH, and k_e of 1.00E-4.

Effect of Humidity Level and Contact Time on Theoretical Breakthrough Curves

The theoretical breakthrough curves at various conditions shown in Figure 5.16 illustrated the same trend and pattern corresponding to the experimental breakthrough curves in Figure 5.8 and 5.9. This indicated that the experimental equilibrium adsorption isotherm considerably played the important role in controlling the adsorption behaviors on the multi-layer adsorber.

Although the breakthrough time calculated from the model was quite shorter than that determined from the experiment, the model could predict the adsorption capacity very accurate as shown in Table 5.3. For this reason, this suggested that under the experimental conditions the model be sufficiently able to predict the breakthrough curves for the adsorption of the water on a multi-layer adsorber.

In each scenario as shown in Table 5.3, the theoretical breakthrough times are 26-29% lower than the experimental values. Moreover, the numbers in all cases appeared quite a constant deviation from the experimental breakthrough time.

Supposed the model was correct, the difference between the theoretical and experimental breakthrough time at the same conditions could occur from the errors in the experiment itself, such as the responding time of the humidity analyzer and its accuracy. Since slow responding time would prolong the breakthrough time. Moreover, the errors might occur from inadequate accuracy of equilibrium adsorption isotherm at low humidity level because no experimental data could be obtained due to the limitations of the apparatus at low humidity level. However, this deviation might occur from the unsatisfied assumption. And also, there were some adsorbents and natural gas properties estimated from the reference book may cause the error of the theoretical breakthrough. The recommendations to accomplish more representative and accurate model will be summarized in CHAPTER VI.

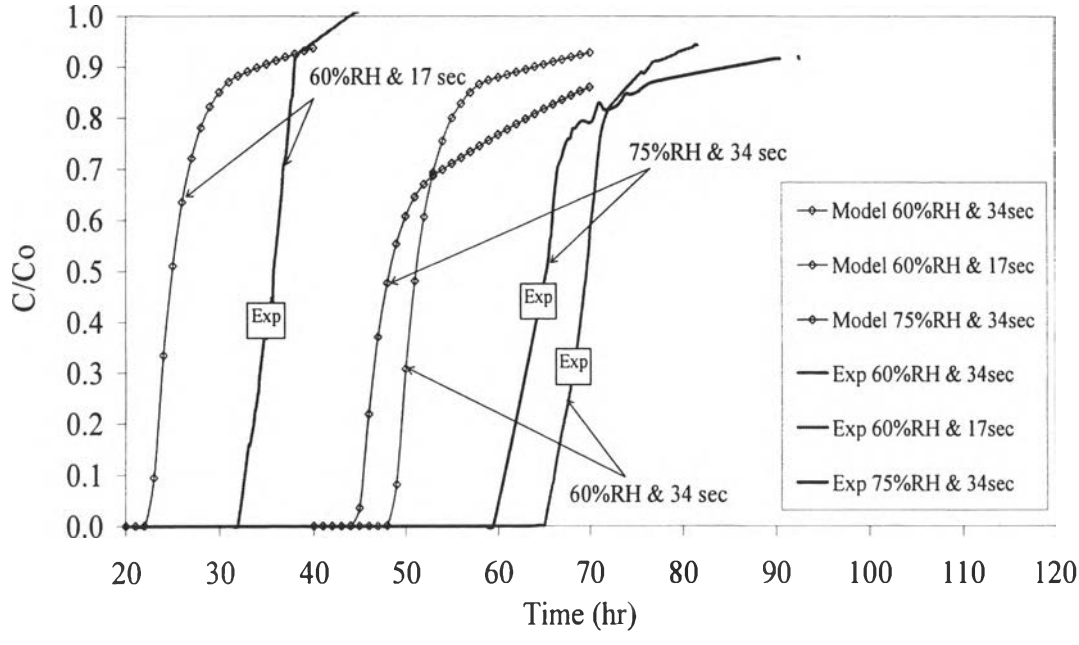

Figure 5.16 Comparison of experimental and theoretical breakthrough curves at various feed humidity and contact time.

Table 5.4 Comparison of adsorption capacity and breakthrough time from the experiments and the mathematical models

Conditions	Adsorption Capacity (g H_2O/100 g adsorbent)			Breakthrough time (hours)		
	Experiment	Model	Error	Experiment	Model	Error
1. 60%RH & CT 34 sec.	21.14	21.91	-3.64%	65.00	48.00	26.15%
2. 75%RH & CT 34 sec.	28.31	27.59	2.54%	59.42	44.02	25.91%
3. 60%RH & CT 17 sec.	22.48	21.66	3.66%	31.90	22.61	29.11%

k_e = 1.00E-4 was used in the model

Characteristic of Breakthrough Curves and Variation of Adsorption Zone with Time

The typical concentration profile in gas phase and adsorbent phase was calculated from the adsorption model. The gas phase concentration, in Figure 5.17, is represented by breakthrough curve while the adsorbent phase concentration, in Figure 5.18, is represented by the mass transfer zone or the adsorption zone.

Figure 5.17 illustrated the breakthrough time with the bed length of 0 to 8.8 cm or the exit of the bed. The graph also illustrates that the breakthrough time keep increasing along the bed length. Eventually, the water concentration in the outlet gas would continue to increase until both water concentrations of the outlet and the inlet gas were the same.

From Figure 5.18, the concentration gradient took place on the adsorbent as referred to the adsorption zone. As the time progressed, the adsorption zone moved deeper downward along the column, and eventually approached the exit of the bed.

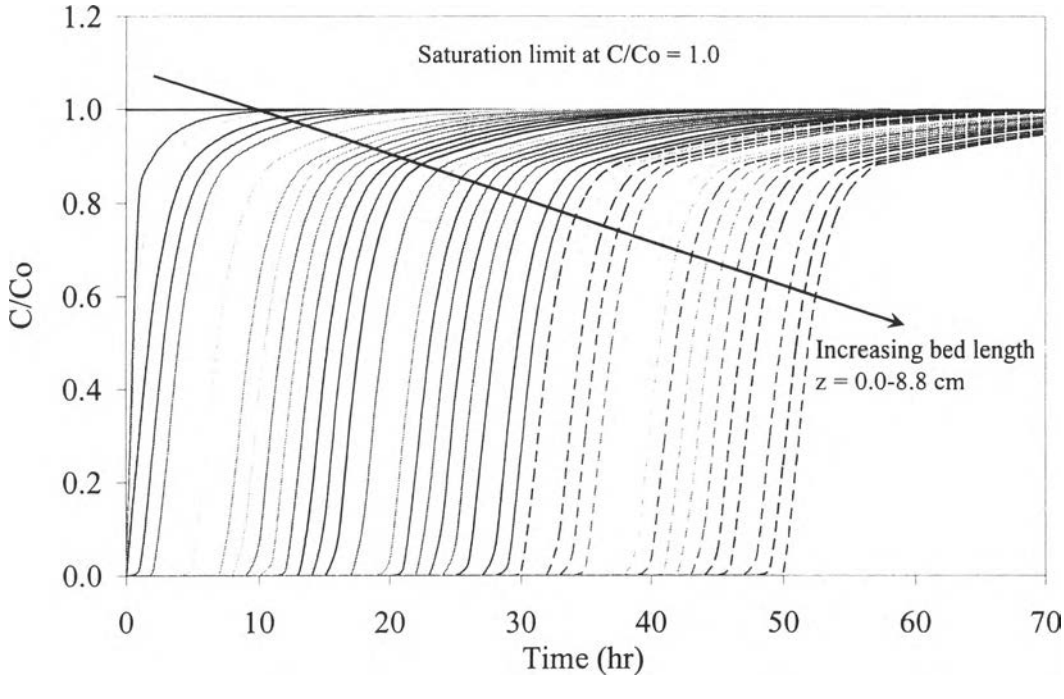

Figure 5.17 Characteristic of breakthrough curves for various adsorption bed lengths at the contact time of 34 sec, the feed humidity of 60%RH, and k_e of 1.51E-4.

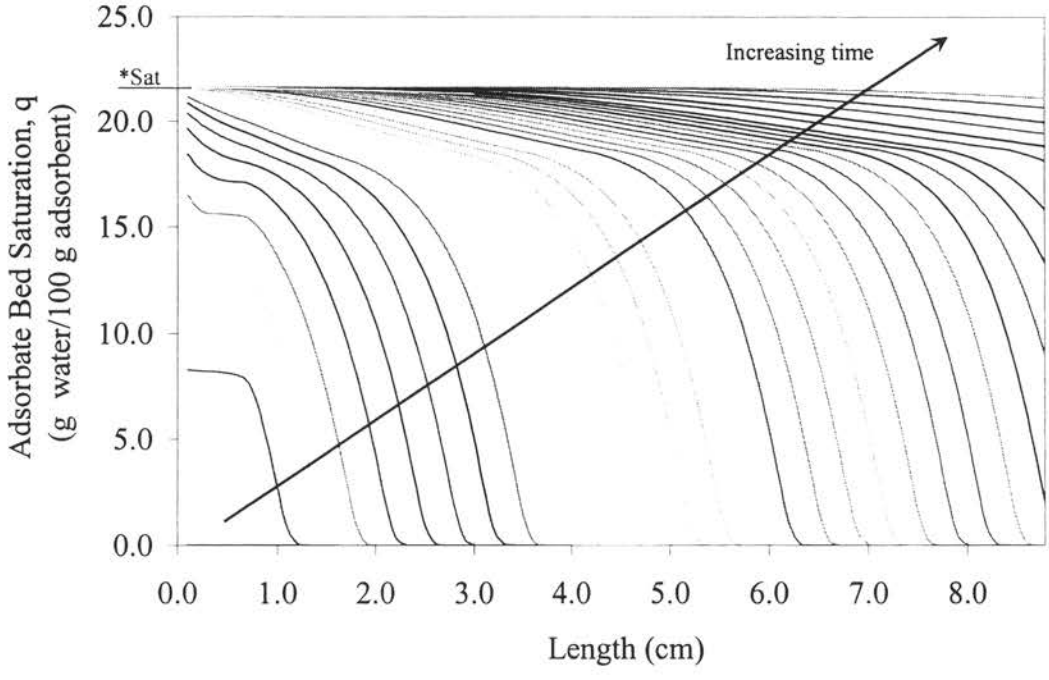

Figure 5.18 Variation of adsorption zone front with time at the contact time of 17 sec, the feed humidity of 60%RH, and k_e of 1.55E-4.